Ceria promotion over Ni-containing hydrotalcite-derived catalysts for CO_2 methane reforming

Radosław Dębek[1,2*], *Monika* Motak[1] , *Maria E.* Galvez-Parruca[2], *Teresa* Grzybek[1], *Patrick* Da Costa[2], and *Ludwik* Pieńkowski[1]

[1]AGH University of Science and Technology, Faculty of Energy and Fuels, Al. A.Mickiewicza 30, 30-059, Kraków, Poland
[2]Sorbonne Universités, UPMC, Univ. Paris 6, CNRS, UMR 7190, Institut Jean Le Rond D'Alembert, 2 Place de la Gare de Ceinture, 78210 Saint-Cyr-L'Ecole, France

Abstract. The catalytic activity in dry methane reforming of hydrotalcite-derived catalysts with ceria and/or nickel species introduced into hydrotalcite interlayer spaces was examined. The prepared materials were characterized (XRF, XRD, FT-IR, H_2-TPR and N_2 sorption) and subsequently tested in CO_2 methane reforming at 550 °C. The obtained results showed that the incorporation of nickel species between hydrotalcite layers resulted in active catalyst with no sign of carbon deposition. Additionally, a beneficial effect of ceria promotion was observed. Ceria-promoted sample exhibited higher activity, stability and selectivity towards DRM, which may be explained by the formation of small Ni crystallites and prevention of the formation of inactive $NiAl_2O_4$ spinel phase.

1 Introduction

The growing emissions of carbon dioxide forced implementation of various CO_2 emission reduction strategies, which may be divided into two main groups: (i) carbon capture and storage (CCS) and (ii) carbon capture and utilization (CCU) technologies [1]. The latter approach allows to convert CO_2 into added-value products, creating in this way a carbon cycle. One of the processes that converts CO_2 into added-value products is dry reforming of methane (DRM). The process leads to an industrially important mixture of H_2 and CO and may be considered an attractive route for syngas production, alternative to the currently applied steam reforming reaction [2]. It may be also applied in Chemical Energy Transmission and/or Storage systems (CETS) for transport and storage of energy [3]. It should be mentioned, however, that DRM process has not yet been commercialized due to the low price of CO_2 emissions, high endothermicity of the reaction and lack of cheap, active and stable catalysts [4].

The investigation for a stable catalyst for DRM process is currently focused on nickel-based materials, as they show similar activity to noble metals but are cheaper and more

* Corresponding author: debek@agh.edu.pl

abundant [5, 6]. However, they still undergo deactivation due to (i) the occurrence of C-forming reactions, which procced easily on large Ni crystallites, and (ii) sintering of nickel active phase. The problem of improving stability of nickel-based catalysts may be solved by increasing nickel-support interactions, which results in the formation of small Ni aggregates and prevents sintering. This may be achieved by the application of appropriate supports. Magnesia and alumina were reported to provide beneficial effects on catalytic performance in DRM due to the formation of NiO-MgO solid solution and $NiAl_2O_4$ spinel phase, respectively [7, 8]. The application of hydrotalcites (layered double hydroxides, HTs) as catalysts precursors for DRM turned out to be of advantage, as all required components i.e. Ni, magnesia and alumina may be introduced into hydrotalcite brucite-like layers [9-11]. In our previous research we showed that hydrotalcite-derived catalysts with nickel introduced into brucite-like layers were promising materials for DRM [12-14].

The other commonly used component of DRM catalyst is ceria. Due to its redox properties, promotion by cerium species may help to oxidize carbon deposits through Boudouard reaction [15, 16]. Moreover, as shown in our previous work, the addition of ceria increases the concentration of intermediate and strong basic sites, which also enhance catalysts stability [17]. Tsyganok et al. [18, 19] proposed an alternative way of introducing nickel species into hydrotalcite structure by co-precipitation in the solution of $[Ni(EDTA)]^{2-}$ complexes.

The work presented in this study was aiming at the comparison of catalytic performance of hydrotalcite-derived materials into which cerium and/or nickel species were introduced into interlayer spaces by co-precipitation in the solution of $[Ce(EDTA)]^{-}$ and/or $[Ni(EDTA)]^{2-}$.

2 Experimental

2.1 Catalyst preparation

The catalysts precursors, hydrotalcite-like materials, were synthesized by co-precipitation method at constant pH from an aqueous solution of appropriate nitrates ($Mg(NO_3)_2 \cdot 6H_2O$, $Al(NO)_3 \cdot 9H_2O$ – Sigma Aldrich) of total cations concentration equal to 1M. The precipitating agent was 1M solution of NaOH (POCH). These two solutions were added simultaneously to the 5wt.% solution of $[Ni(EDTA)^{2-}]$ or mixture of 5 wt.% $[Ni(EDTA)^{2-}]$ and 3 wt.% $[Ce(EDTA)^{-}]$, resulting in samples HTNi and HTNi-Ce, respectively. An additional reference material was synthesized by co-precipitation in 0.05 M solution of Na_2CO_3 (sample HTMgAl). The flows of various solutions were adjusted in order to maintain constant pH equal to 10. The co-precipitation was carried out under constant stirring at 65 °C. The obtained mineral suspension was aged at 65 °C for 1h and subsequently washed with warm distilled water (ca. 50-60 °C) and filtered until neutral pH of the filtrate was registered. The synthesized materials were dried in air overnight at 80 °C and ground into fine powder. Finally, prepared hydrotalcites were calcined in the stream of air (10 cm^3/min) at 550 °C for 4 h.

2.2 Physico-chemical characterization

The chemical composition of prepared catalysts was examined by X-ray fluorescence (XRF). The measurements were carried out in an energy dispersive XEPOS spectrometer from Spectro Ametek. X-ray diffraction (XRD) patterns were recorded on an Empyrean diffractometer from PANalytyical, in the 2Θ ° using a Cu X-ray source (λ=1.5046 Å). Textural properties were evaluated from the N_2 adsorption isotherms acquired at -196 °C in

a Belsorp Mini II equipment. Prior to each measurement, the samples were outgassed at 120 °C for 3 h. Temperature-programmed reduction (TPR) profiles were recorded with a BELCAT-M apparatus from BEL Japan, equipped with a thermal conductivity detector (TCD). The samples (ca. 50 mg) were first degassed at 100 °C for 2 h, then reduced at 7.5 °C/min using 5 % H_2 in Ar. Fourier Transform Infrared Spectroscopy (FT-IR) measurements were carried out on Frontier spectrometer from PerkinElmer. The sample was diluted in KBr in relation 1:10 and subsequently DRIFT spectra were recorded in the range of 4000-450 cm^{-1}.

2.3 Catalytic tests

The activity towards DRM of the synthesized hydrotalcite-derived materials was tested in a fixed-bed reactor. Prior to the experiments, each catalyst was reduced with hydrogen (5 % H_2 in Ar) at 900 °C. The catalytic tests were carried out at 550 °C for 5 h with the substrate molar ratio $CH_4/CO_2/Ar=1/1/8$ and GHSV equal to 20,000 h^{-1}. The total gas flow was equal to 100 cm^3/min. The products of the reaction were analysed by gas chromatography (490 Varian Micro-GC).

3 Results and discussion

3.1 Physicochemical characterization of the prepared materials

Designation of the prepared catalysts and their chemical composition are presented in Table 1. The coprecipitation of hydrotalcites in the solution of $[Ni(EDTA)^{2-}]$ complexes resulted in incorporation of ca. 7 wt.% of nickel and for HTNi-Ce sample around 3 wt.% of cerium. The calculated values of M^{2+}/M^{3+} molar ratios for prepared materials were very close to the nominal ones (Table 1), pointing to the successful synthesis of HTs materials with a desired composition.

Table 1 The designation of the prepared catalysts and their chemical composition determined by XRF.

Sample	Cations in brucite-like layers	Species present in interlayer spaces	Ni (wt.%)	Mg (wt.%)	Al (wt.%)	Ce (wt.%)	M^{2+}/M^{3+}
HTNi	Mg^{2+}, Al^{3+}	Ni^{2+}	7.7	18.4	7.1	-	2.9 (3)*
HTNi-Ce	Mg^{2+}, Al^{3+}	Ni^{2+}, Ce^{3+}	7.2	17.9	7.5	3.2	3.1 (3)*
HTMgAl	Mg^{2+}, Al^{3+}	-	-	37.4	14.15	-	2.9 (3)*

* in the parenthesis are given nominal values

The XRD diffractograms recorded for the prepared catalysts are depicted in Fig. 1. The freshly prepared materials (Fig. 1A) exhibited reflections characteristic for the 3R rhombohedral layered structure of hydrotalcite (ICOD 00-014-0191). The reference sample (HTMgAl) showed reflections at 2Θ equal to ca. 11, 23 and 35 °, arising from the diffraction of X-rays on (003), (006) and (009) planes [20]. In case of samples HTNi and HTNi-Ce the shift of the first reflections to lower values of 2Θ was observed (reflections at ca. 6, 12, 18, 24 °). The position of the first reflections in hydrotalcites XRD patterns is dependent on the basal spacing between layers, and thus the type of anions present between hydrotalcite layers. The shift of the first reflections observed for samples HTNi and HTNi-Ce may be thus explained by incorporation of $[Ce(EDTA)^{-}]$ and/or $[Ni(EDTA)^{2-}]$ anions

into interlayer spaces. The similar shift of the first reflection position to 2Θ ca. 6 ° was observed by Tsyganok et al. [18].

All samples exhibited rhombohedral symmetry, thus parameter *c* of unit cell may be calculated from the position of the first reflection or by averaging the positions of the first three reflections, and unit cell parameter *a* from the position of the first reflection from the doublet present at 2Θ equal to ca. 61° [21]. The calculated parameters are presented in Table 2. The parameter *a*, which describes average cation-cation distances in the brucite-like layers, had the same value for all samples, indicating that the incorporation of cerium and/or nickel species into interlayer spaces did not affect layered structure. The parameter *c*' (c'=*c*/3), which describes basal spacing in hydrotalcite structure, increased for HTNi and HTNi-Ce samples with respect to the reference HTMgAl material, pointing to the successful incorporation of cerium and/or nickel species into hydrotalcite structure.

Materials after calcination (Fig. 1B) exhibited reflections (2Θ ca. 43 and 63 °) characteristic for periclase-like mixed oxides, which is typical for the products of HTs thermal decomposition [22]. Additionally, HTNi-Ce sample showed the presence of CeO_2 phase (reflection at 2Θ ca. 30 °).

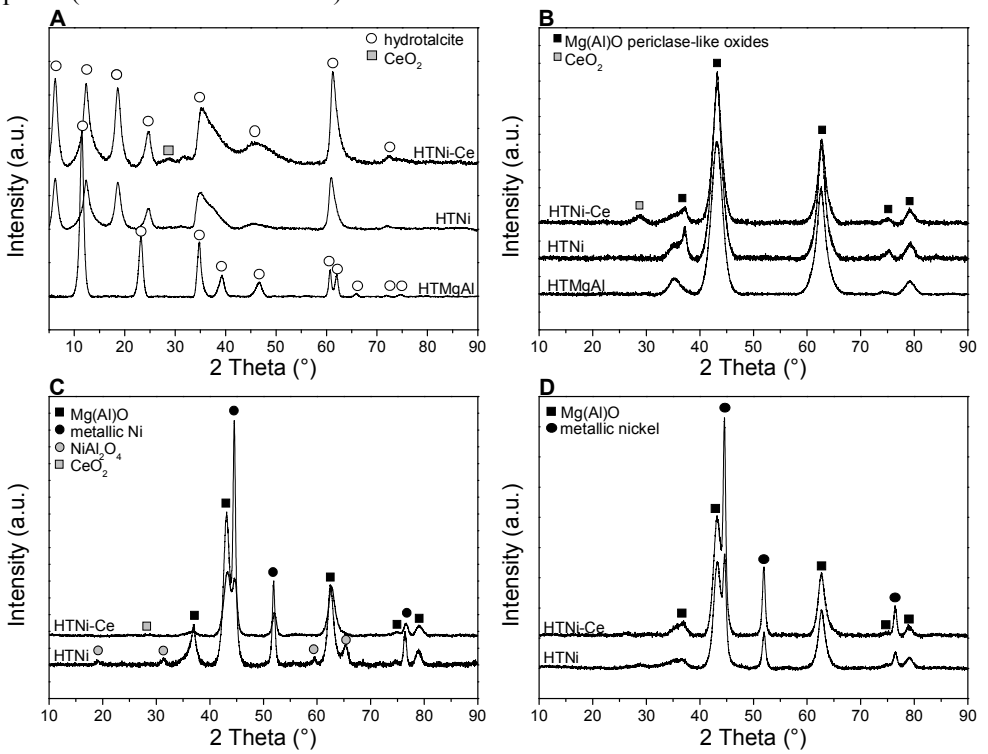

Fig. 1 The XRD diffractograms for: (A) freshly prepared hydrotalcites, (B) calcined materials, (C) reduced samples, (D) catalysts after 5 h DRM catalytic tests at 550 °C

The FT-IR spectra recorded for freshly prepared hydrotalcites are presented in Fig. 2A. All samples exhibited a number of common absorption bands observed at 3550, 3000, 1650, 1370 and 870 cm^{-1}. The broad band at 3550 cm^{-1} arises from the stretching vibration of structural OH^- groups in the metal hydroxide layer [20]. A small shoulder at ca. 3000 cm^{-1} may be attributed to a second type of OH^- stretching vibrations of interlayer hydrogen bonding with carbonate groups. The weak band at 1650 cm^{-1} was ascribed to interlayer water molecules. The strong band at 1370 cm^{-1} and weak band at 870 cm^{-1}, were attributed to the stretching vibration and out-of-plane bending vibration of CO_3^{2-} [23]. The bands in

the range of 450-700 cm^{-1} are typical of the frameworks of HTs, and indicate M-OM stretching, which further confirms that the catalysts precursors are ordered hydrotalcites [24]. The presence of a weak band at ca. 1376 cm^{-1} may be indicating the presence of NO_3^- anions [25], and is in good agreement with the value of *c*' parameter calculated from XRD measurements for sample HTMgAl (Table 2).

Table 2 The unit cell parameters, anions present in the interlayer spaces and textural properties of synthesized hydrotalcites (S_{BET} – specific surface area, V_{tot} – total volume of pores; d_r – mean pore diameter).

Sample	Unit cell parameter		Anions in interlayer spaces	S_{BET} (m^2/g)	V_{tot} (cm^3/g)	d_r (nm)
	a (Å)	*c*'=c/3 (Å)				
HTNi	3.06	14.12	$[Ni(EDTA)^{2-}]$	231	0.36	6
HTNi-Ce	3.06	14.23	$[Ni(EDTA)^{2-}]$ and $[Ce(EDTA)^-]$	229	0.38	6
HTMgAl	3.06	7.84	CO_3^{2-} and NO_3^-	95	0.87	35

Samples HTNi and HTNi-Ce exhibited additionally absorption bands associated with EDTA molecules. The band at 2930 and 2850 cm^{-1} are ascribed to asymmetric and symmetric C-H stretching of methylene groups. The absorption of infrared radiation by asymmetric stretching of coordinated and uncoordinated COO^- may be attributed to the bands at 2850 and 1600 cm^{-1}, respectively, while band at 1110 cm^{-1} to the vibration of C-N single bonds [18, 24]. These results agree with the XRD measurements which confirmed the presence of nickel-EDTA and Ce-EDTA chelates between brucite-like layers for samples HTNi and HTNi-Ce.

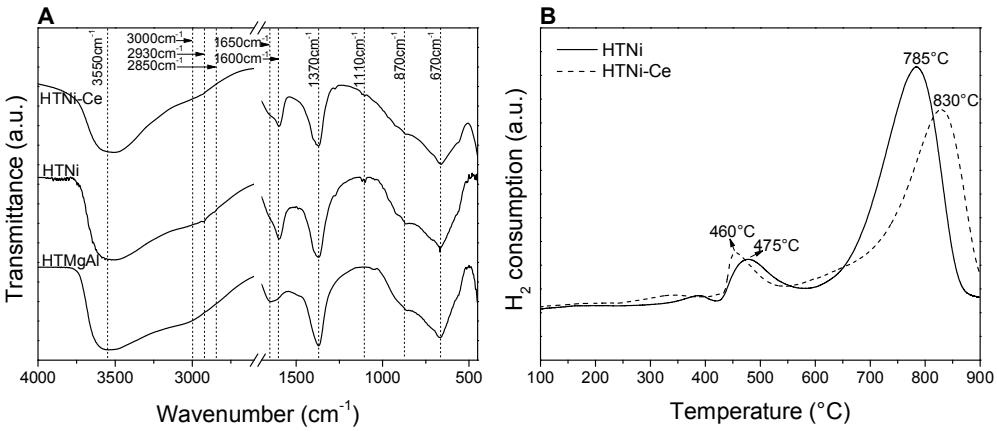

Fig. 2 FT-IR spectra (A) and H_2-TPR profiles (B) for the prepared materials.

H_2-TPR profiles recorded for Ni-containing samples are depicted in Fig. 2B. Both samples exhibited the presence of two types of Ni species, suggesting various types of interactions between NiO species and the mesoporous Mg(Al)O support. According to literature, pure NiO phase is reduced at the temperature range 220-420 °C [26-28]. Thus the reduction peaks centered at 460 and 475 °C for HTNi-Ce and HTNi, respectively, might be attributed to the reduction of NiO weakly bonded with support surface. The most intense reduction peak was observed for both catalysts between 600 and 900 °C, indicating strong interactions between nickel species and support. These peaks may be thus attributed to the reduction of Ni^{2+} in NiO-MgO solid solution or $NiAl_2O_4$ spinel phase, which were formed upon calcination [13, 24].

The introduction of ceria species between HTs brucite-like layers modified H_2-TPR profile. The position of the reduction peaks was shifted and additionally small reduction peak centred at ca. 340 °C appeared. The explanation of the reduction process of sample HTNi-Ce is quite complicated, as the reduction profiles of NiO and ceria may be overlapping. As described in literature, the reduction of CeO_2 occurs in three stages: (i) reduction of surface oxygen or oxygen capping species (around 300 °C) [29], (ii) reduction of surface lattice oxygen (450-600 °C) [15] and (iii) total bulk reduction (up to 900 °C) [9]. Therefore, the peak observed at 340 °C and the shift of the peak in the 400-500 °C region may be attributed to the overlapping reduction profiles of NiO and CeO_2. The most intense peak was shifted to higher temperatures (from 785 to 830 °C), indicating that the addition of ceria decreased reducibility of nickel species and suggesting increased metal-support interactions for the Ce-promoted catalyst. This results stay in line with the estimated Ni crystallite sizes for the reduced samples basing on XRD results (Table 3, Fig. 1C).

The values of textural parameters calculated for the prepared catalysts basing on N_2 sorption experiments are presented in Table 2, and corresponding sorption isotherms and distribution of pores are depicted in Fig. 3. The samples exhibited specific surface areas between 100-230 m^2/g, in agreement with the data reported in literature for similar hydrotalcite-derived materials [18, 20, 24]. Samples HTNi and HTNi-Ce showed much higher values of S_{BET} with respect to the reference material (HTMgAl), which was caused by the substitution of carbonate anions by [$Ce(EDTA)^-$] and/or [$Ni(EDTA)^{2-}$] complexes. This resulted in the increase of basal spacing between hydrotalcite layers, as confirmed by XRD. The shape of N_2 adsorption isotherm and the distribution of pores for HTNi and HTNi-Ce samples also differed. Narrow pores and the shape of adsorption/desorption isotherm suggest the formation of microporous materials. Moreover the observed hysteresis loop was of type H4, pointing to the uniform distribution of slit shaped pores [30]. This clearly indicates that the type of anions present in the interlayer spaces of hydrotalcite has a strong influence on textural properties of the studied catalysts. However, the introduction of cerium species did not affect textural properties of prepared material with respect to the HTNi sample.

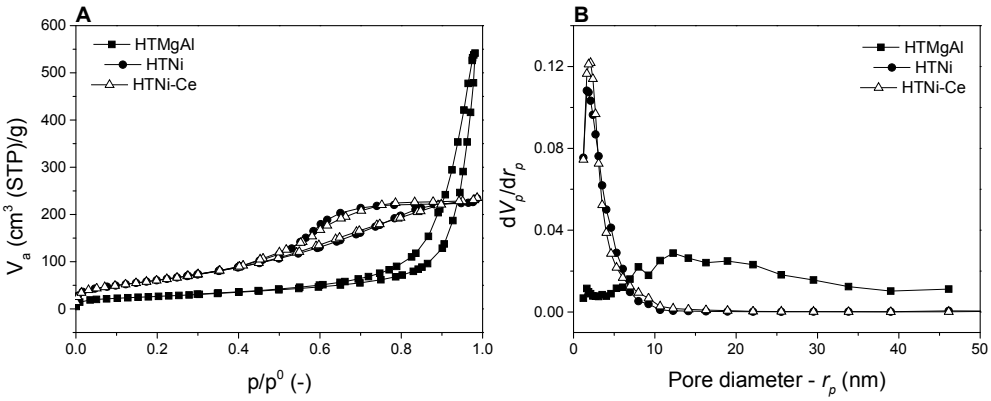

Fig. 3 N_2-adsorption/desorption isotherms (A) and pore diameter distribution (B) of the studied materials.

3.2 Low temperature CO_2 reforming of methane

The synthesized materials were tested in low temperature CO_2 methane reforming reaction at 550 °C (Fig. 4). At temperature as low as 550 °C, the Ni-containing hydrotalcite-derived materials showed good catalytic performance. The catalytic activity towards both CH_4 and

CO_2 was higher for ceria-promoted sample and reached values of ca. 30 and 37 %, respectively. Both catalysts showed higher conversions of CO_2 than those of CH_4, indicating the occurrence of reverse water gas shift reaction (RWGS). This is directly reflected in the distribution of obtained products, as an excess of carbon monoxide was observed for both catalysts (Fig. 4B). The CO_2 conversions were decreasing with the time on stream (TOS), pointing to deactivation of the catalysts. On the other hand, the opposite trend was registered for CH_4 conversions.

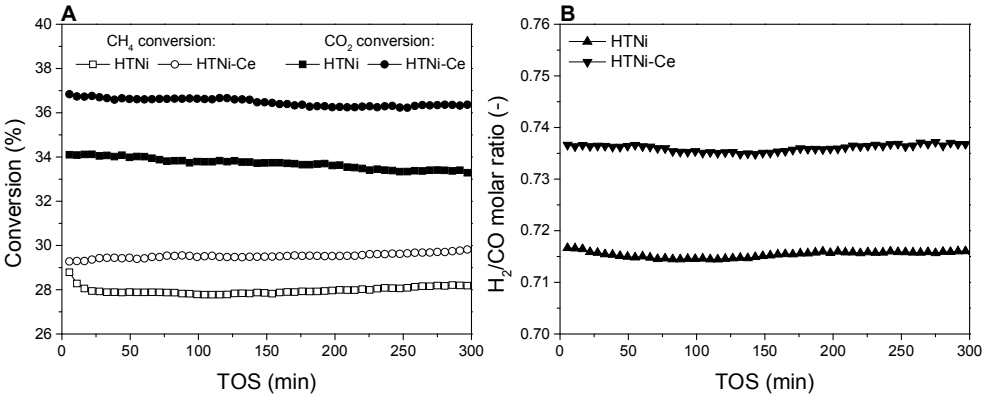

Fig. 4 The results of catalytic tests: (A) CH_4 and CO_2 conversions (B) H_2/CO molar ratio; temperature 550 °C; CH_4/CO_2/Ar=1/1/8; GHSV=20,000 h^{-1}; total flow 100 cm^3/min;

The beneficial effect of ceria addition on catalysts activity may be explained by the fact that Ce-promoted sample had smaller Ni crystallites with an average size of ca. 8 nm (Table 3). Small Ni crystallites are desired in dry reforming process, as it allows to avoid C-forming side reactions which proceed more easily on large Ni crystallites [31]. Therefore, sample HTNi-Ce was more selective towards DRM which resulted in higher activity and higher selectivity.

Another possible explanation of the beneficial effect of ceria addition is that sample HTNi exhibited formation of $NiAl_2O_4$ spinel phase after reduction in H_2 (Fig. 1C). As reported in literature, the formation of spinel phase has a negative effect on catalysts activity towards DRM, as nickel species in $NiAl_2O_4$ are too strongly bonded with the support and thus cannot be reduced during catalyst activation. As a result, lower amount of metallic nickel species is formed [31, 32]. Therefore the addition of Ce species, by modifying reducibility of NiO, prevents the formation of inactive spinel phase.

Table 3 The Ni crystallite size estimated for the reduced and spent catalysts after DRM at 550 °C.

Sample	Ni crystallite size* (nm)	
	Reduced samples	Catalyst after DRM tests
HTNi	12	13
HTNi-Ce	8	8

*estimated by Scherrer equation

The catalysts after reaction were analysed by XRD experiments (Fig. 1D). Both catalysts did not exhibit any graphitic carbon (reflection at 2Θ equal to ca. 26°). On the other hand, such type of carbon deposit was observed for Ni-containing hydrotalcite-derived catalyst with nickel species introduced into HTs brucite-like layers. It originated from direct CH_4 decomposition [14]. These results indicate that the incorporation of Ni species between brucite-like layers results in the catalyst resistant to the methane decomposition. This explanation is in good agreement with the obtained values of H_2/CO

molar ratio (Fig. 4B). However, the formation of amorphous carbon on HTNi and HTNi-Ce catalysts cannot be excluded and further characterization is required for further confirmation. Basing on XRD experiments for the reduced and spent catalysts Ni crystallite sizes were estimated (Table 3). No sintering of Ni active phase was observed after 5h TOS. The Ce-promoted catalyst exhibited smaller Ni crystallites, which may explain more stable performance with respect to HTNi catalyst.

4 Conclusions

The hydrotalcite-derived materials were synthesized and tested in DRM reaction. Nickel species were introduced into HTs-based catalytic system at the co-precipitation stage, resulting in the incorporation of Ce and/or Ni species into hydrotalcite interlayer spaces. The obtained results showed that the method of nickel introduction influenced material properties, especially their texture. The prepared catalysts turned out to be active in low temperature dry reforming. Higher activity, stability and selectivity towards DRM was exhibited by ceria-promoted sample, indicating the beneficial effects of ceria addition. the formation of small Ni crystallites upon catalyst reduction in H_2. Additionally, Ce-promoted sample did not exhibit the formation of inactive $NiAl_2O_4$ spinel phase, which enhanced its catalytic performance.

The obtained results showed that the method of nickel and ceria introduction into HTs-based catalytic systems strongly influenced their catalytic properties. As reported in literature, the introduction of ceria and nickel onto hydrotalcite surface and into brucite-like layers, respectively, resulted in increased reducibility of NiO. However, it did not affect the size of Ni crystal size [9, 15, 33]. Therefore, the application of the appropriate method of catalysts synthesis may allow tailoring their catalytic properties in dry reforming reaction.

The work was financed within NCBiR strategic research project ‘Technologies supporting development of safe nuclear energy’, research task no. 1 ‘Development of high temperature reactors for industrial applications’, agreement no. SP/J/166183/12, step task no. 15 ‘Preparation and physicochemical characterization of catalysts for dry reforming of methane’.
R. Dębek and M. Motak would like to acknowledge AGH grant 11.11.210.213.

References

1. A.J. Hunt, E.H.K. Sin, R. Marriott, J.H. Clark, Generation, Capture, and Utilization of Industrial Carbon Dioxide, Chemsuschem, 3 (2010) 306-322.
2. J.-M. Lavoie, Review on dry reforming of methane, a potentially more environmentally-friendly approach to the increasing natural gas exploitation, Frontiers in Chemistry, 2 (2014).
3. J.T. Richardson, S.A. Paripatyadar, Carbon dioxide reforming of methane with supported rhodium, Applied Catalysis, 61 (1990) 293-309.
4. N. Thybaud, Lebain, D., , Panorama des vois de valorisation du CO_2, French Agence de l'Environnement et de la Maitrise de l'Energie, Angers, France, 2010.
5. M.S. Fan, A.Z. Abdullah, S. Bhatia, Catalytic Technology for Carbon Dioxide Reforming of Methane to Synthesis Gas, Chemcatchem, 1 (2009) 192-208.
6. M. Usman, W.M.A. Wan Daud, H.F. Abbas, Dry reforming of methane: Influence of process parameters—A review, Renewable and Sustainable Energy Reviews, 45 (2015) 710-744.
7. A. Becerra, M. Dimitrijewits, C. Arciprete, A. Castro Luna, Stable Ni/Al_2O_3 catalysts for methane dry reforming, Granular Matter, 3 (2001) 79-81.

8. R. Zanganeh, M. Rezaei, A. Zamaniyan, Dry reforming of methane to synthesis gas on NiO–MgO nanocrystalline solid solution catalysts, Int J Hydrogen Energ, 38 (2013) 3012-3018.
9. C.E. Daza, J. Gallego, J.A. Moreno, F. Mondragón, S. Moreno, R. Molina, CO_2 reforming of methane over Ni/Mg/Al/Ce mixed oxides, Catal Today, 133–135 (2008) 357-366.
10. A.R. Gonzalez, Y.J.O. Asencios, E.M. Assaf, J.M. Assaf, Dry reforming of methane on Ni-Mg-Al nano-spheroid oxide catalysts prepared by the sol-gel method from hydrotalcite-like precursors, Appl Surf Sci, 280 (2013) 876-887.
11. O.W. Perez-Lopez, A. Senger, N.R. Marcilio, M.A. Lansarin, Effect of composition and thermal pretreatment on properties of Ni–Mg–Al catalysts for CO_2 reforming of methane, Applied Catalysis A: General, 303 (2006) 234-244.
12. R. Dębek, K. Zubek, M. Motak, P. Da Costa, T. Grzybek, Effect of nickel incorporation into hydrotalcite-based catalyst systems for dry reforming of methane, Res Chem Intermediat, 41 (2015) 9485-9495.
13. R. Dębek, K. Zubek, M. Motak, M.E. Galvez, P. Da Costa, T. Grzybek, Ni–Al hydrotalcite-like material as the catalyst precursors for the dry reforming of methane at low temperature, Comptes Rendus Chimie, 18 (2015) 1205-1210.
14. R. Dębek, M. Motak, D. Duraczyska, F. Launay, M.E. Galvez, T. Grzybek, P. Da Costa, Methane dry reforming over hydrotalcite-derived Ni-Mg-Al mixed oxides: the influence of Ni content on catalytic activity, selectivity and stability, Catalysis Science & Technology, 6 (2016) 6705-6715.
15. C.E. Daza, S. Moreno, R. Molina, Co-precipitated Ni–Mg–Al catalysts containing Ce for CO_2 reforming of methane, Int J Hydrogen Energ, 36 (2011) 3886-3894.
16. C.E. Daza, C.R. Cabrera, S. Moreno, R. Molina, Syngas production from CO_2 reforming of methane using Ce-doped Ni-catalysts obtained from hydrotalcites by reconstruction method, Applied Catalysis A: General, 378 (2010) 125-133.
17. R. Dębek, M. Radlik, M. Motak, M.E. Galvez, W. Turek, P. Da Costa, T. Grzybek, Ni-containing Ce-promoted hydrotalcite derived materials as catalysts for methane reforming with carbon dioxide at low temperature - On the effect of basicity, Catal Today, 257 (2015) 59-65.
18. A.I. Tsyganok, K. Suzuki, S. Hamakawa, K. Takehira, T. Hayakawa, Mg–Al Layered Double Hydroxide Intercalated with $[Ni(edta)]^{2-}$ Chelate as a Precursor for an Efficient Catalyst of Methane Reforming with Carbon Dioxide, Catal Lett, 77 (2001) 75-86.
19. A.I. Tsyganok, T. Tsunoda, S. Hamakawa, K. Suzuki, K. Takehira, T. Hayakawa, Dry reforming of methane over catalysts derived from nickel-containing Mg-Al layered double hydroxides, J Catal, 213 (2003) 191-203.
20. F. Cavani, F. Trifirò, A. Vaccari, Hydrotalcite-type anionic clays: Preparation, properties and applications, Catal Today, 11 (1991) 173-301.
21. V. Rives, Characterisation of layered double hydroxides and their decomposition products, Materials Chemistry and Physics, 75 (2002) 19-25.
22. D. Tichit, B. Coq, Catalysis by Hydrotalcites and Related Materials, CATTECH, 7 (2003) 206-217.
23. S. Kannan, A. Dubey, H. Knozinger, Synthesis and characterization of CuMgAl ternary hydrotalcites as catalysts for the hydroxylation of phenol, J Catal, 231 (2005) 381-392.
24. P. Tan, Z. Gao, C. Shen, Y. Du, X. Li, W. Huang, Ni-Mg-Al solid basic layered double oxide catalysts prepared using surfactant-assisted coprecipitation method for CO_2 reforming of CH_4, Chinese Journal of Catalysis, 35 (2014) 1955-1971.

25. E. Lopez-Salinas, Y. Ono, Intercalation chemistry of a Mg□Al layered double hydroxide ion-exchanged with complex MCl2−4 (M □ Ni, Co) ions from organic media, Microporous Materials, 1 (1993) 33-42.
26. C. Li, Y.-W. Chen, Temperature-programmed-reduction studies of nickel oxide/alumina catalysts: effects of the preparation method, Thermochimica Acta, 256 (1995) 457-465.
27. B. Mile, D. Stirling, M.A. Zammitt, A. Lovell, M. Webb, The location of nickel oxide and nickel in silica-supported catalysts: Two forms of "NiO" and the assignment of temperature-programmed reduction profiles, J Catal, 114 (1988) 217-229.
28. A. Kadkhodayan, A. Brenner, Temperature-programmed reduction and oxidation of metals supported on γ-alumina, J Catal, 117 (1989) 311-321.
29. K.Y. Koo, S.-h. Lee, U.H. Jung, H.-S. Roh, W.L. Yoon, Syngas production via combined steam and carbon dioxide reforming of methane over Ni–Ce/$MgAl_2O_4$ catalysts with enhanced coke resistance, Fuel Processing Technology, 119 (2014) 151-157.
30. G. Leofanti, M. Padovan, G. Tozzola, B. Venturelli, Surface area and pore texture of catalysts, Catal Today, 41 (1998) 207-219.
31. Y.H. Hu, E. Ruckenstein, Catalytic Conversion of Methane to Synthesis Gas by Partial Oxidation and CO_2 Reforming, Advances in Catalysis, Academic Press2004, pp. 297-345.
32. Y.-g. Chen, J. Ren, Conversion of methane and carbon dioxide into synthesis gas over alumina-supported nickel catalysts. Effect of Ni-Al_2O_3 interactions, Catal Lett, 29 (1994) 39-48.
33. H.-P. Ren, Y.-H. Song, W. Wang, J.-G. Chen, J. Cheng, J. Jiang, Z.-T. Liu, Z.-W. Liu, Z. Hao, J. Lu, Insights into CeO_2-modified Ni–Mg–Al oxides for pressurized carbon dioxide reforming of methane, Chemical Engineering Journal, 259 (2015) 581-593.